OPEN ACCESS

GAVIN PUBLISHERS

Advance Research on Foot and Ankle

Research Article

Al-Mulla M, et al. Adv Res Foot Ankle: ARFA-110.

DOI: 10.29011/ ARFA-110.1000010.

Quality Assurance Phantom Testing of an Echo-Planar Diffusion-Weighted Sequence on a 3T Scanner

Muna Al-Mulla[1*], Allison McGee[2], Patrick Kenny[3], Louise Rainford[4]

[1]Department of Health Sciences, University of Kuwait, Kuwait

[2]University College Dublin School of Medicine and Medical Science, Health Sciences Centre, University College Dublin, Belfield, Dublin 4, Ireland

[3]Department of Radiology, Mater Misericordiae University Hospital, Level 2, The Whitty Building, North Circular Road, Dublin 7. Ireland

[4]University College Dublin School of Medicine and Medical Science, Health Sciences Centre, University College Dublin, Belfield, Dublin 4, Ireland

[*]**Corresponding author:** Muna Al-Mulla, Department of Health Sciences, University of Kuwait; Email: muna@HSC.EDU.KW

Citation: Al-Mulla M, McGee A, Kenny P, Rainford L (2019) Quality Assurance Phantom Testing of an Echo-Planar Diffusion-Weighted Sequence on a 3T Scanner. Adv Res Foot Ankle: ARFA-110. DOI: 10.29011/ ARFA-110.1000010.

Received Date: 10 December, 2018; **Accepted Date:** 10 January,2019; **Published Date:** 18 January, 2019

Abstract

Purpose: This work investigated the behaviour of a high-field MR system relative to a range of pulse sequence parameter changes and image artefacts resulting from image acquisition employing an Echo-Planar Diffusion-Weighted (EPI-DW) sequence modified for musculoskeletal imaging of the Achilles Tendon (AT).

Methods and Materials: MR scanning was undertaken on a 3T Philips Achieva MR scanner with an 8-channel foot/ ankle coil. Image quality evaluation was based on images acquired using two phantoms: 1) an L-shaped foot/ ankle phantom containing Nickel Chloride (NiCl2) in water and 2) a small cylindrical plastic phantom containing copper sulphate (CuSO4) in water. Quality control (QC) measurements were based on the American College of Radiology (ACR) specifications. Signal-to-noise ratio (SNR), image intensity uniformity, percentage ghosting, and geometric distortion were measured for phantom images acquired using four sequences (T1W SE, T2W TSE, STIR, EPI-DW).

Results: The performance of the EPI-DW sequence was tested according to ACR specifications and compared to three standard pulse sequences routinely used for scanning of the AT. The EPI-DW sequence met the ACR criteria for SNR and image intensity uniformity, but failed to meet geometric distortion criteria. In terms of percentage ghosting, artefacts were evident in the EPI-DW and ADC map images. However, when quantified, these images remained within ACR specifications for image ghosting.

Conclusion: When modifying a pulse sequence for a new application, it is essential to understand in advance the technical performance characteristics of the MR system and their potential impact on resultant MR image quality. This study demonstrated that the results of image quality testing revealed important findings that facilitated further optimisation of the EPI-DW sequence prior to its application for Achilles tendon scanning in human subjects.

Keywords: Imaging; Image processing; Magnetic resonance imaging; Phantoms; Quality Control; EPI; DWI

Introduction

Over the past few years Magnetic Resonance Imaging (MRI) has rapidly developed in both clinical practice and research. High field strength MR scanners (i.e., 3 Tesla) have enabled new pulse sequences and advanced imaging techniques to be applied in clinical practice, making MR image acquisition faster, diverse and more sensitive to pathology [1,2]. High field systems have facilitated the application of a wider range of pulse sequences in routine clinical practice rather than limiting them principally to the research arena. In this context, the application of Diffusion-Weighted Imaging (DWI) has expanded from an MR imaging technique used exclusively for neuroimaging to applications in the body and musculoskeletal

system [3]. DWI is a technique that measures the thermal motion of molecules within tissues. When coupled with an Apparent Diffusion Coefficient (ADC) map, DWI can be used to generate quantitative values representing pathological changes associated with various diseases [4]. The principal application of DWI is in brain imaging for the assessment of infarct and stroke-related pathology; however, more recently it is being increasingly and routinely used for tumour staging, size measurements and morphological characteristics [4]. However, with advanced sequences such as DWI, which is based on Echo-Planar Imaging (EPI), it has become increasingly challenging to maintain high image quality to facilitate accurate depiction of anatomy and pathological changes. MR images generated using an EPI-DWI sequence may suffer from an inherent low Signal-To-Noise Ratio (SNR) and can be very sensitive to several types of artefacts such as blurring or motion; some of which may be sufficiently severe to hinder the extraction of accurate quantitative Apparent Diffusion Coefficient (ADC) values [5]. MR systems are susceptible to technical problems due to the complex, interrelated demands on the system to maintain high-performance imaging [6]. Artefacts (e.g. eddy current, motion, ghosting and chemical shift) in MRI can be the result of several factors, including: magnetic field imperfections that are not normally visible, scanner hardware or software limitation or malfunction, or as a consequence of the characteristics of the subject scanned [7]. Although techniques have been developed to reduce these artefacts, not every artefact can be avoided or minimized, with some being very unpredictable and difficult to overcome [1]. Several authors have acknowledged the complexity of those artefacts resulting from the use of high-field systems to acquire certain types of advanced sequences, one of such is the EPI-DWI discussed in this paper [2,7]; and have advocated the application of Quality Control (QC) testing in the clinical setting specifically for this sequence. Standard QC tests can help maintain MR system performance, facilitate the recognition of the source of defects within MR images, and enable analysis and tuning of MR system performance. In QC testing, the focus is on optimising MR system characteristics such as spatial resolution (ghosting), linearity (geometric distortion), homogeneity (image intensity uniformity), and signal (signal-to-noise ratio) [8,9]. Routine QC phantom scanning can either be performed weekly and/ or monthly at each site, and tends to be based on visual inspection of the MR images. However, [10] has indicated that this approach is insufficient for the EPI-DWI sequence, which is prone to inconsistencies in measured values for some of the above indices of MR image quality. Given the resultant difficulties evaluating artefact severity across a number of EPI-DW images, stand-alone testing was recommended together with quantitative evaluation of image quality indices This study aimed to demonstrate the impact of performing MR phantom scanning and quantifying the results using a computer-based approach for QC measurements in the development of a new sequence for application in a clinical study. The technical characteristics and artefacts associated with the acquisition of an EPI-DWI sequence modified for ankle joint imaging images on a 3T MR scanner were explored. These findings enabled parameter optimisation prior to application of this sequence for Achilles tendon scanning on human subjects.

Materials and Methods

A multi-step QC testing process was undertaken to compare the performance of the EPI-DWI sequence against a series of standard pulse sequences routinely used for musculoskeletal MR imaging. The methodology was approved by the local Research Ethics Committee. Four indices of MR image quality were evaluated using the methodology for phantom scanning and evaluation proposed by the ACR (American College of Radiology) [11]: geometric distortion (aspect ratio), Signal-To-Noise Ratio (SNR), image intensity uniformity, and percentage signal ghosting. Values for each of these indices, as recommended by the ACR, are outlined in (Table 2).

MR System and Phantom Specifications

Phantom MR imaging was undertaken on a 3 Tesla Philips Achieva scanner with the following gradient characteristics: 40mT/m, 200mT/m/msec and incorporating an integrated 8-element, SENSE phased array Radiofrequency (RF) coil dedicated for foot/ ankle imaging (Figure 1c). The parameters for the standard sequences: T_1W Spin Echo (SE), Turbo Spin Echo (TSE), Short Tau Inversion Recovery (STIR) and the EPI-DW sequence tested are presented in Table 1. All phantom images were acquired in the axial orientation.

The two phantoms provided by the MR scanner vendor, were kept at room temperature prior to scanning and had the following characteristics:

a) 31.8 mm/L Nickel Chloride in water ($NiCl_2$-H_2O), L-shaped to fit inside the dedicated foot/ ankle RF coil (Figure 1a);

b) 770 mg of Copper Sulphate ($CuSO_4$) in water contained within a small, cylindrical plastic bottle (Fig 1b)

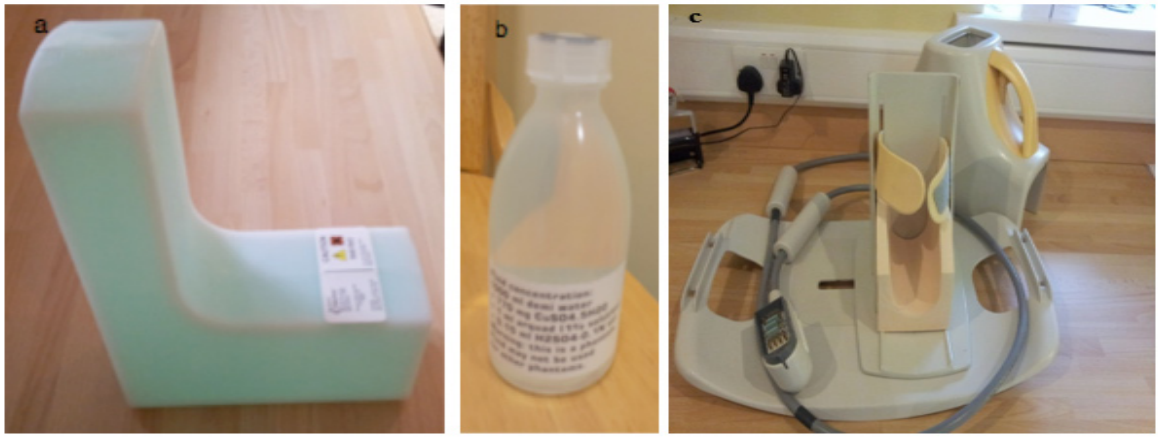

Figure 1: MR phantoms; (a) L-shaped Nickel Chloride ($NiCl_2$) in water (b) Cylindrical bottle containing a solution of Copper Sulphate ($CuSO_4$) in water, and the foot/ ankle RF coil (c) used for QC testing.

Sequence Parameter	TR (ms)	TE (ms)	Slice Thickness (mm)	NEX (Avg)	Number of Slices	Parallel Imaging	Matrix
T_1-W SE	400	12	3	4	15	No	256x320
T_2-W TSE	4500	81	3	4	15	No	218x320
STIR	3800	46	3	4	15	No	269x384
EPI-DW (b-values: 0; 40; 273; 800)	2030	30	3	12	15	SENSE	112x526

Table 1: Imaging parameters for the phantom scans.

Axial images of the $NiCl_2$ phantom were first acquired using, in order, a T1W SE, T2W FSE, STIR and EPI-DWI sequence to test for geometric distortion (aspect ratio), Signal-To-Noise Ratio (SNR), image intensity uniformity, and percentage signal ghosting. For consistency, each sequence was acquired twice using sameparameters (Table 1). To correct for artefact resulting from using a diffusion-weighted sequence, measurements were repeated using the $CuSO_4$ phantom to evaluate image intensity uniformity and SNR.

MR system specifications and Image Acquisition

MR Phantom Image Analysis

The acquired DICOM-format MR images of the phantoms were processed and analysed using Matlab (Math Works, Inc.) and according to the ACR specifications for aspect ratio (geometric distortion), Signal-To-Noise Ratio (SNR), image intensity uniformity and percentage signal ghosting (Table 2). Geometric distortion of all sequences was determined by using aspect ratio (e.g. measurement of width to height), then comparing the aspect ratio (true dimension) of the curved-border of the L-shaped MR phantom to that of the scanned images (observed measurement). The MR phantom and all sequence measurements were taken at 90° to each other, with mean height and length values recorded to provide the vertical and horizontal extent of the target object within the (axial) MR images (Figure 2). Once an aspect ratio was determined, the percent distortion was calculated using the formula from (Table 2).

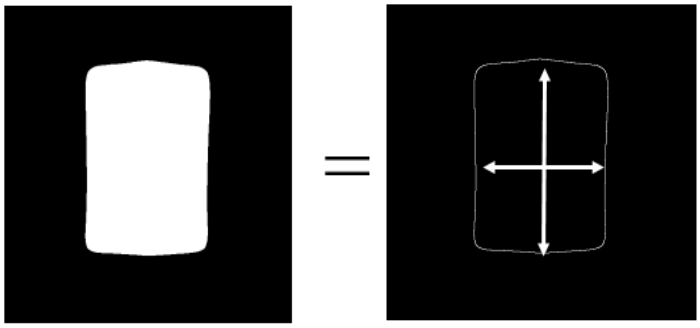

Figure 2: The phantom is an L-shaped square with calculations at 90° angles (white arrows) undertaken using Matlab software to measure mean values corresponding to the four boundaries to provide the vertical and horizontal extent of the target object. Percentage Image Uniformity (PIU) was calculated using the Region-Of-Interest (ROI) measurement tool to determine the mean signal intensity of 70% within the interior region of the $NiCl_2$ phantom target object (Table 2). Regions of maximum (S_{Max}) and minimum (S_{Min}) signal intensity, typically 0.5% (1 cm^2), were located within images acquired using each of the sequences evaluated (Figure 3). Mean signal intensity measurements (PIU) were calculated according this formula (Table 2).

Criteria	ACR Acceptance Criteria	Formula	Images
Geometric Distortion	Percent distortions in the are generally considered acceptable if they are < 5%	$\%\ GD = \frac{\text{True dimensions} - \text{observed dimension}}{\text{True dimensions}}\ x100\%$	Figure 2
Image Intensity Uniformity (PIU)	PIU should be greater than or equal to 90% for MRI systems with field strength of 3 Tesla.	$PIU = 100\ X\left[1 - \frac{(High - Low)}{(High + Low)}\right]$	Figure 3
Signal To Noise Ratio (SNR)	The SNR value is dependent on SNR meet or exceed the values provided by the coil manufacturer (high SNR)	$SNR = \frac{Mean\ Signal}{SD\ Background\ Noise}$	Figure 4
Percent-Signal Ghosting	Ghosting ratio should be ≤0.025	$Ghosting = \left\lvert\frac{([Top + Bottom] - [Left + Right])}{2x(Object)}\right\rvert$	Figure 5

Table 2: Criteria used for evaluating the phantom images obtained using the four pulse sequences mentioned in (Table 1).

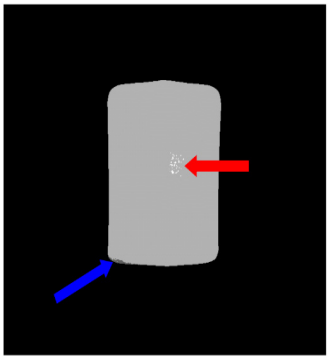

Figure 3: An image demonstrating regions of maximum and minimum signal intensity. The ROI has been placed at what was visually estimated to be the largest 1 cm^2 dark area (blue arrow), the ROI was placed at what was visually estimated to be the brightest 1 cm^2 (red arrow), following the ACR specification for calculation.

SNR was determined by isolating the target object in the MR images using a threshold value derived from the histogram (Figure 4) of the pixel value frequency. In each case, a minimum pixel value between the distributions for object and background was selected as the global threshold value [9]. A value for noise was estimated as the mean value of the background pixels, excluding zero-value pixels. Using measurement tools available through Matlab software on the standard PC used for quantitative phantom image analysis, the interior 75% of the target was located using a morphological 'close' operation and the mean pixel value of this region represented the mean signal intensity of the phantom. The SNR was then obtained by dividing the standard deviation of the outside ROI from the mean of the inside ROI (formula Table 2)

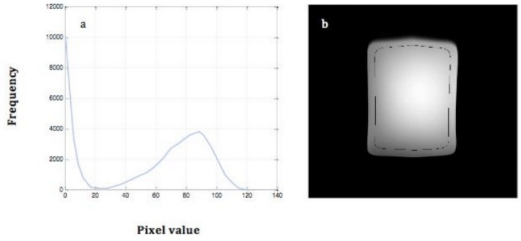

Figure 4: Images show the method used to measure Signal-To-Noise Ratio (SNR) using Matlab software automated for SNR calculation. The target object in the image was isolated using a threshold value derived from the histogram (a) of pixel value frequency. The interior 75% (b) of the target was located using a morphological 'close' operation and the mean pixel value of this region represented signal value.

A measure of ghosting ratio was derived according to ACR recommendations. The mean signal from the phantom (object) was obtained from within a large target Region-Of-Interest (ROI) that was more than 70% of the cross-sectional area of the phantom. Mean signals were also taken from the image background in the frequency-encoding direction (Top + Bottom) and in the phase-encoding direction (Left + Right) (Figure 5). Areas of each rectangular region outside the phantom target were approximately 10% of the size of the interior of the target object. The ghosting ratio was calculated using these rectangular regions located approximately halfway between the phantom object and image boundaries in the respective directions using the formula in (Table 2).

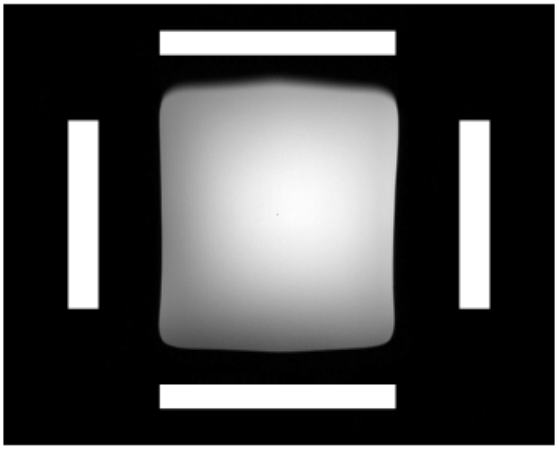

Figure 5: Image displaying a measure of ghosting ratio, derived from the ACR approach, where the target object is 70% of the interior of the phantom, and the rectangles outside this target located top, bottom, left & right in the respective frequency- and phase-encoding directions.

Data from the Matlab and OsiriX software were then transferred to the Statistical Package for Social Sciences (IBM SPSS version 20.0 Inc.) to facilitate calculation of mean and standard deviation values and histogram analysis of all four image quality indices for the phantom MR images acquired using the T1-W SE, T_2-W TSE, STIR and EPI-DW sequences (Table 3). ADC maps of quantitative diffusion measurements taken were generated using OsiriX software for MAC, incorporating an added software plugin. Using its "Grow Region", 3D segmentation and "ROI Volume" functional options, mean and Standard Deviation (SD) ADC values were measured from the EPI-DW scans (scan 1 and scan 2, as each sequence was acquired twice) (Tables 4,5).

Sequence	Geometric Distortion (Aspect Ratio) Mean ± (SD)	Percent-Signal Ghosting	Image Intensity Uniformity Mean ± (SD)	Signal-To-Noise Ratio Mean ± (SD)
T_2W Scan 1	1.25 ± (0.07)	0.001± (0.004)	51.43 ± (0.62)	16.6 ± (0.061)
T_2W Scan 2	1.25 ± (0.07)	0.001 ± (0.003)	51.57 ± (0.84)	16.60 ± (0.03)
T_1W Scan 1	1.26 ± (0.07)	0.000 ± (0.000)	56.13 ± (1.05)	228.91 ± (26.93)
T_1W Scan 2	1.25 ± (0.07)	0.000 ± (0.000)	55.80 ± (0.73)	233.50 ± (27.26)
STIR Scan 1	1.24 ± (0.08)	0.002 ± (0.003)	60.28 ± (1.92)	36.38 (2.39)
STIR Scan 2	1.24 ± (0.08)	0.003 ± (0.003)	60.21 ± (1.33)	45.98 ± (3.53)
EPI-DW b=0 Scan 1	1.11 ± (0.16)	0.011 ± (0.003)	65.58 ± (1.95)	79.17 ± (8.37)
EPI-DW b=0 Scan 2	1.13 ± (0.18)	0.013 ± (0.003)	64.19 ± (2.51)	71.53 ± (6.23)
EPI-DW b=40 Scan 1	1.11 ± (0.16)	0.011 ± (0.003)	66.96 ± (2.24)	76.91 ± (8.08)
EPI-DW b=40 Scan 2	1.13 ± (0.17)	0.013 ± (0.003)	66.65 ± (2.64)	64.51 ± (4.98)
EPI-DW b=273 Scan 1	1.12 ± (0.17)	0.010 ± (0.003)	66.04 ± (2.26)	65.61 ± (4.86)
EPI-DW b=273 Scan 2	1.14 ± (0.17)	0.013 ± (0.003)	65.11 ± (2.34)	56.86 ± (3.49)
EPI-DW b=800 Scan 1	1.13 ± (0.17)	0.010 ± (0.006)	63.17 ± (1.90)	34.66 ± (2.96)
EPI-DW b=800 Scan 2	1.14 ± (0.17)	0.013 ± (0.006)	62.61 ± (2.72)	28.31 ± (2.42)

Table 3: QC Test Results for the L-shaped MR Phantom.

Sequence	Apparent Diffusion Coefficient (ADC) Values		
	$Nicl_2$ in Water Phantom Scan 1 Mean ± SD × 10^{-3} [Mm^2/S]	**$Nicl_2$ in Water Phantom Scan 2 Mean ± SD × 10−3 [Mm^2/S]**	**$Cuso_4$ in Water Phantom Scan 1 Mean ± SD × 10^{-3} [Mm^2/S]**
EPI-DW b=0	2.1 ± (0.066)	2.1 ± (0.059)	2.0 ± (0.038)
EPI-DW b=40	2.0 ± (0.373)	2.0 ± (0.363)	2.0 ± (0.047)
EPI-DW b=273	2.0 ± (0.109)	2.1 ± (0.109)	2.0 ± (0.039)
EPI-DW b=800	2.1 ± (0.060)	2.1 ± (0.069)	2.0 ± (0.048)

Table 4: Apparent diffusion coefficient measurements for the $NiCl_2$ and $CuSO_4$ in water MR phantoms.

Sequence	Image Intensity Uniformity $Cuso_4$ In Water Phantom Mean ± (SD)	Signal To Noise Ratio $Cuso_4$ In Water Phantom Mean ± (SD)	Image Intensity Uniformity $Nicl_2$ In Water Phantom Mean ± (SD)	Signal To Noise Ratio $Nicl_2$ In Water Phantom Mean ± (SD)
EPI-DW B=0	91.7 ± (1.5)	446.18 ± (44.6)	64.88 ± (2.23)	75.35 ± (7.3)
EPI-DW B=40	90.3 ± (1.3)	440.35 ± (34.34)	66.80 ± (2.44)	70.71 ± (6.53)

EPI-DW B=273	91.3 ± (1.3)	282.03 ± (22.28)	65.57 ± (2.3)	61.23 ± (4.17)
EPI-DW B=800	89.2 ± (1.1)	98.68 ± (7.27)	62.89 ± (2.31)	31.48 ± (2.69)

Table 5: Image quality indices for the EPI-DW sequence derived from images of Copper Sulphate ($CuSO_4$) and Nickel Chloride ($NiCl_2$) in water phantoms.

Results

To determine geometric distortion, aspect ratio measurements for the $NiCl_2$ L-shaped phantom were calculated using the formula:

$$Aspect\ ratio = \frac{Width}{Hight} = \frac{7.923}{6.045} = 1.31\ cm$$

According to the ACR criteria specifications, percentile values calculated from images acquired using each of the pulse sequences is considered acceptable if they are < 5%. All routine sequences T_1W SE (3.8%), T_2W TSE (4.5%), and STIR (5%) passed the specification criteria for geometric distortion. While, the EPI-DW sequence; b=0 (14%), b=40 (14%), b=273 (12.5%), b=800 (12.5%) failed to remain within the desired criteria, scoring higher than the desired < 5% for acceptable geometric distortion. In terms of image intensity uniformity, images acquired using the STIR and DW-EPI sequences achieved the highest scores across the four sequences evaluated. However, none of the sequences achieved the ACR recommended value of 90-100% image intensity uniformity when measured from the MR $NiCl_2$ phantom images. When this index of image quality was re-evaluated for the images acquired using the $CuSO_4$ based phantom, the performance of the EPI-DWI sequence improved, achieving image intensity uniformity values well within the ACR-recommended range: (Mean / SD) b=0 (91.7 / 1.5); b=40 (90.3 / 1.3); b=273 (91.3 / 1.3), b=800 (89.2 / 1.12). Relative to percentage signal ghosting, this was found not to be of significance for the images acquired for all sequences evaluated. However, images acquired using the EPI-DW sequence achieved the highest score for this image quality index indicating a higher prevalence of ghosting artefact (Table 3). According to ACR the acceptance criteria for SNR measurements could not be specified in general terms since the values are MR imaging system specific and dependent on other factors such as: RF coil characteristics, scanning conditions, phantom T_1 and T_2 values etc. However, variations were noted in the SNR values calculated for the sequences tested, with images acquired using the T1W SE sequence scoring highest (228.91), and those acquired using the T2W TSE sequence achieving the lowest score (16.6) (Table 3). The EPI-DW sequence performed well, achieving the second highest score after the T1W SE sequence using the $NiCl_2$ phantom, with b=0 images scoring higher than those for b=800 (Table 3). Conversely, the EPI-DW images scored the highest measured SNR using the $CuSO_4$ phantom (b=0 [446.18], b=40 [440.35], b=273 [282.03], b=800 [98.68]), compared to SNR measured using the $NiCl_2$ phantom (b=0 [75.35], b=40 [70.71], b=273 [61.23], b=800 [31.48]) (Table 4). According to Numano [12], the diffusion coefficient of pure water at 20°C is 2.023 × 10^{-3} mm^2/s. In this work, the ADC values calculated from the EPI-DW images are summarised in (Table 4). ADC measurements for the phantom were found to be consistent with literature, with minimal variation related to temperature and concentration of water to Nickel Chloride of the MR phantom at the time of scanning [3,12].

Discussion

The QC tests performed provided a simple and comprehensive assessment of the performance of an EPI-DW sequence modified for Achilles tendon scanning. All image quality related characteristics of the acquired phantom MR images were quantitatively evaluated.

Geometric Distortion

ACR specifications for acceptable geometric distortion suggest that the absolute value for percentage geometric distortion calculated using the formula in (Table 2) should not exceed 5% [11]. MR system performance for this study, based on measurements of the MR phantom and MR phantom images was such that the standard T1W SE, T2W TSE and STIR sequences were all within ACR specifications for geometric distortion. However, when using the EPI-DW sequences, MR phantom images failed to meet ACR specifications, scoring higher than the specified 5%. The scoring of the images acquired using the EPI-DW sequence in terms of aspect ratio was 1.11 to 1.14, according to the different b-values used, while the actual aspect ratio of the MR phantom was 1.3, indicating a scoring difference of 12-14% from the true dimension, i.e., the true value. In general, the American Association of Physicists in Medicine (AAPM) indicate that a failure in a geometric distortion test can be attributed to gradient non-uniformity, as the linearity of the gradient magnetic field is the principal hardware factor affecting geometric accuracy [9]. However, as only the EPI-DW sequence failed the ACR geometric distortion specification a more sequence-specific factor is implicated. According to Ardekani & Sinha [13], Echo-Planar Imaging (EPI) based diffusion-weighted image acquisition suffers from geometric distortions due to both local magnetic field in homogeneities and eddy current effects that arise from the large diffusion gradients required to obtain diffusion-weighted images. Thus, the distortion artefact is related to the composition of the DW sequence, specifically the EPI-based acceleration technique. These authors [13] then further explain that when using EPI techniques coupled with a DW sequence there are inevitable trade-off factors inherent to EPI, of which the most

noteworthy is the higher sensitivity to susceptibility-induced magnetic field distortions. Literature recommends the use of field map correction, short-axis readout, and parallel imaging acceleration techniques to reduce geometric distortion artefacts for an improved quality of the EPI-DW acquisition [14]. Identification of geometric distortion in EPI-DW images is important, specifically for MSK MR scanning because of the variation in tissue composition (e.g. bone, fat, fluid), which makes identification of artefacts such as. motion, eddy current and shimming failure complex [7].

Percent Signal Ghosting

In this study, the degree of image ghosting was quantified under the assumption that no motion occurred within the MR phantom images as movement was reduced by using padding during image acquisition, and MR system vibration was minimal. The ACR specifies that for ghosting artefact to be image acceptable it should measure less than or equal to 0.025. From (Table 3) it is evident that images acquired using all the routine pulse sequences and the EPI-DW sequence acquired at low b-values (b=0, 273, 400) passed the ACR criteria for signal ghosting. However, images acquired using the EPI-DW sequence with a high b-value (b=800) displayed minimal signal ghosting. According to Bammer et al [15], different b-values can influence the degree of ghosting artifact, which was evident from the results for the EPI-DW sequence. The use of a high b-value is necessary to detect variations in pathology from minor tissue degradation to complete destruction of the Achilles tendon [16]. Thus, it is essential to understand the underlying reason for the ghosting artefact in order to implement the correct technique to eliminate it. Since ghosting was more prominent in the images acquired using the EPI-DW sequence at high b-values of 800, it was concluded that this artifact occurred as a result of the influence of DW and EPI in combination within the sequence. A number of steps can be implemented to eliminate ghosting artefact related to the EPI-DW sequence several including: the application of inner volume shims and more complete spectral fat suppression (Spectral Attenuated Inversion Recovery SPIR or SPAIR), which are possible to apply on the 3T scanners.

Image Intensity Uniformity

According to literature [17,9,11] the common causes of poor sequence performance in an image intensity uniformity test include incorrect phantom positioning, ghosting, and RF coil failure. According to ACR guidelines, the Percentage Intensity Uniformity (PIU) for MR scanners operating at field strengths greater than 2T is expected to be between 90-100%. However, if using water-filled phantoms at field strengths at or above 3T, the dielectric and penetration effects are more prevalent and a figure of less than 90% intensity uniformity is acceptable. In this study, all sequences tested failed to meet the ACR specification for image intensity uniformity. Sobol [18] has suggested a reason for this based on a study in which five different 3T MR scanners were tested for image intensity uniformity using the ACR acquisition and measurement protocol, but failed to meet the required value. This may be related to the RF properties of the ACR phantom due to limitations imposed by the electromagnetic physics and the resonant RF frequency of 3T MRI systems. Furthermore, since the focus of this research involved testing the quality of images acquired using an EPI-DW sequence, a plastic cylindrical bottle filled with Copper Sulphate solution was used to re-test the image intensity uniformity (Table 5). EPI-DW images scores determined using the images from this $CuSO_4$-based phantom were within 90% of the ACR specification for percentage image intensity uniformity, indicating poor compliance for images acquired using the phantom comprising Nickel Chloride in solution. The AAPM indicate that water-filled phantoms as described above are not optimal for acceptance QA testing of high-field scanners due to RF penetration and dielectric effects that become more pronounced with increasing frequency [9]. To avoid obtaining low image intensity uniformity values for such high-field systems, Alecci et al [19] recommend the use of oil-based QA phantoms, which minimise the dielectric and penetration effects that occur at field strengths of 3T and above.

Signal-to-Noise-Ratio

An important advantage when scanning at high magnetic field strength is the increased MR signal generated [20]. This increased signal is particularly useful when optimising SNR for DWI sequences acquired at different b-values, and specifically high b-values, which tend to reduce the inherent SNR [4]. However, this magnitude of SNR increase is not attained in practice because SNR is influenced by several factors including: physiological noise, scanner hardware characteristics, Radio-Frequency (RF) field inhomogeneity and increased susceptibility effects [21]. Furthermore, SNR also depends on the metabolite concentration comprising the QA phantom and the T_1 / T_2 relaxation times of the metabolites [22]. While changes in T_1 relaxation time with increasing field strength are well understood, the effects of the higher magnetic field strength on T_2 relaxation times are not as predictable. Cochlin & Blamire [22] further explain that T_1 and T_2 are largely independent of each other: T_1 principally determined by the amount of paramagnetic ions present and T_2 primarily a function of the MR phantom concentration. This is seen in a study performed by Li & Mirowitz [23] in which different phantom concentrates were used and in all scans T_2 scored less than T_1. Similarly, a study by Chien-Chuan et al [24] involving QA testing of five different 3T scanners, found that SNR for T2W sequences in all the tests performed was lower than for the T_1W sequences. For the STIR sequence Li & Mirowitz [23], explain that STIR is robust at all field of strengths and may be less vulnerable to field inhomogeneity, though it often produces lower SNR. Furthermore, given the many MR system characteristics upon which SNR depends, acceptance criteria for SNR cannot be specified in general terms since the values will always be system specific [24]. This is evident in the results for this study, as consistent with literature evidence, variation in SNR measurements for all four sequences was noted (Figure 6). For further confirmation of SNR behaviour and its dependency on different parameters was evident when the EPI-DW sequence was

re-tested with a phantom containing a Copper sulphate solution, demonstrating an increase in the measured SNR (Table 5). Li & Mirowitz [25] explained this in terms of the inherent sensitivity of EPI to magnetic susceptibility effects. Susceptibility artefacts may be mitigated through the use of parallel imaging, which has been shown to be particularly successful when used in association with EPI-DW sequences [26].

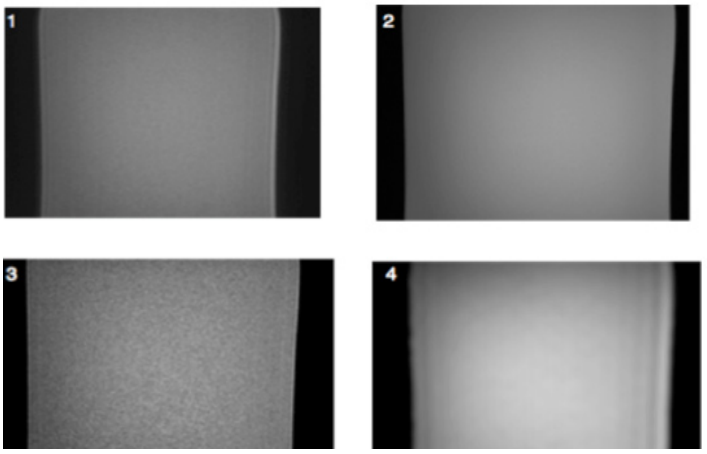

Figure 6: Images of the Nickel Chloride ($NiCl_2$) in water MR phantom displaying visual differences in SNR for: 1. STIR, 2. T_1W SE, 3. T_2W TSE, and 4. EPI-DW sequences.

Apparent Diffusion Coefficient

ADC represents a valuable biomarker of disease; thus, ADC quantitative measurements are necessary for validation and calibration of EPI-DW sequences [27]. According to Graessner [3], ADC is very dependent on temperature, with pure water having a diffusion coefficient of 3 x 10^{-3}mm^2/s at body temperature, which serves as a standard for MR scanners. However, the phantoms used in this study did not contain pure water and the mean ambient room temperature was 19˚C. Changes in the calculated ADC values may be attributed to these variations together with some ghosting artifact that influences overall image uniformity.

Conclusion

3T imaging availability is increasing within healthcare systems. The advantages of such high-field scanners have been well documented for several clinical applications including neuro imaging, MR angiography and MR imaging of the small anatomical structures comprising the joints. However, a number of image artefacts are more prominent at 3T. Understanding their physical origin can help radiographers and MR scientists to manage these artefacts through pulse sequence and image protocol optimisation and testing in advance of commencing clinical MR imaging of volunteer and/or patient subjects. Applying phantom testing of the EPI-DW sequence to be used for Achilles tendon imaging as part of a subsequent clinical study inferred important information regarding the behaviour of the 3T MR scanner and the RF coil relative to ACR-defined measurements of MR image quality.

Advances in Knowledge

The results of this study are of relevance for research and clinical testing of EPI-DW pulse sequences with ADC map measurements on high-field 3T MR scanners. This study facilitated the continuation to a study designed to measure qualitative DWI and quantitative ADC measurement of the Achilles tendon and related pathology.

Acknowledgement

Special thanks to, Mr. David Costello MSc. Medical Physicist (Mater Misericordiae University Hospital), and, Ms. Annette White MR Clinical Specialist Radiographer (Cappagh National Orthopaedic Hospital).

References

1. Tanenbaum LN (2006) Clinical 3T MR imaging: mastering the challenges. Magn Reson Imaging Clin N Am 4: 1-15.
2. Schmitt F, Grosu D, Mohr C, Purdy D, Salem K, et al. (2004) 3 Tesla MRI: successful results with higher field strengths. Radiologe 44: 31-47.
3. Graessner J (2011) Frequently Asked Questions: Diffusion-Weighted Imaging (DWI). MAGNETOM Flash 84-87.
4. Luna A, Ribes R, Soto JA (2012) Diffusion MRI outside the brain. Berlin: Springer.
5. Liu Z, Wang Y, Gerig G, Gouttard S, Tao R, et al. (2010) Quality Control of Diffusion Weighted Images. Proc Soc Photo Opt Instrum Eng 11: 7628.
6. Ihalainen TM, Lonnroth NT, Peltonen JI, Uusi-Simola JK, Timonen MH, et al. (2011) MRI quality assurance using the ACR phantom in a multi-unit imaging center. Acta Oncologica 50: 966-972.
7. Le Bihan D, Poupon C, Amadon A, Lethimonnier F (2006) Artifacts and pitfalls in diffusion MRI. J Magn Reson Imaging 24: 478-488.
8. Bushberg J (2012) The essential physics of medical imaging. Philadelphia; Wolters Kluwer Health/Lippincott Williams & Wilkins.
9. Jackson EF, Bronskill MJ, Drost DJ, Och J, Pooley RA, et al. (2010) American Association of Physicists in Medicine. Acceptance Testing and Quality Assurance Procedures for Magnetic Resonance Imaging Facilities. AAPM REPORT NO. 100, American Association of Physicists in Medicine, Houston: American Association of Physicists in Medicine One Physics Ellipse.
10. Delakis I, Moore EM, Leach MO, DE Wilde JP (2004) Developing a quality control protocol for diffusion imaging on a clinical MRI system. Phys Med Biol 49: 1490-1422.
11. American College of Radiology. Phantom test guidance for the ACR MRI accreditation program. Reston: American College of Radiology, 2005.
12. Numano T, Hyodo K, Nitta N, Hata J, Iwasaki N, et al. (2004) Apparent Diffusion Coefficient Mapping Using a Multi-Shot Spiral MRI Sequence of the Rat Brain. Open Journal of Radiology 4: 13-24.

13. Ardekani S, Sinha U (2005) Geometric distortion correction of high-resolution 3 T diffusion tensor brain images. Magn Reson Med 54: 1163-1171.

14. Chang HC, Chuang TC, Lin YR, Wang FN, Huang TY, et al. (2013) Correction of geometric distortion in Propeller echo planar imaging using a modified reversed gradient approach. Quant Imaging Med Surg 3: 73-81.

15. Bammer R, Augustin M, Prokesch RW, Stollberger R, Fazekas F (2002) Diffusion-weighted imaging of the spinal cord: interleaved echo-planar imaging is superior to fast spin-echo. J Magn Reson Imaging 15: 364-373.

16. Khoo MM, Tyler PA, Saifuddin A, Padhani AR (2011) Diffusion-weighted imaging (DWI) in musculoskeletal MRI: a critical review. Skeletal Radiol 40: 665-681.

17. Chen CC, Wan YL, Wai YY, Liu HL (2004) Quality assurance of clinical MRI scanners using ACR MRI phantom: preliminary results. J Digit Imaging 17: 279-84.

18. Sobol W (2006) Some Issues with Image Intensity Uniformity Test Performed On 3T MRI Scanners. Med Phys 33: 2209-2210.

19. Alecci M, Collins C, Smith M, Jezzard P (2001) Radio Frequency Magnetic Field Mapping of a 3 Tesla Birdcage Coil: Experimental and Theoretical Dependence on Sample Properties. Magnetic Resonance in Medicine 46: 379-385.

20. Schmitz BL, Aschoff AJ, Hoffmann MH, Gron G (2005) Advantages and Pitfalls in 3T MR Brain Imaging: A Pictorial Review. AJNR Am J Neuroradiol 26: 2229-2237.

21. Chang K, Kamel I (2010) Abdominal imaging at 3T: challenges and solutions. Applied Radiology 39: 22-31.

22. Cochlin L, Blamire A, Styles P (2003) Dependence of T_1 and T_2 on high field strengths in doped agarose gels; facilitating selection of composition for specific T_1/T_2 at relevant field. Proc. Intl. Soc. Mag. Reson 11: 885.

23. Li T, Mirowitz SA (2002) Comparative study of fast MR imaging: quantitative analysis on image quality and efficiency among various time frames and contrast behaviours. Magn Reson Imaging 20: 471-478.

24. National Electrical Manufacturers Association. Determination of Signal-to-Noise Ratio (SNR) in Diagnostic Magnetic Resonance Imaging. 2008. National Electrical Manufacturers Association, Rosslyn (VA), USA: NEMA Standards Publications MS 1- 2008.

25. Li T, Mirowitz SA (2003) Fast T_2-weighted MR imaging: impact of variation in pulse sequence parameters on image quality and artifacts. Magn Reson Imaging 21: 745-753.

26. Skare S, Newbould RD, Clayton DB, Albers GW, Nagle S, et al. (2007) Clinical multishot DW-EPI through parallel imaging with considerations of susceptibility, motion, and noise. Magn Reson Med 57: 881-890.

27. Matsuya R, Kuroda M, Matsumoto Y, Kato H, Matsuzaki H, et al. (2009) A new phantom using polyethylene glycol as an apparent diffusion coefficient standard for MR imaging. Int J Oncol 35: 893-900.